

TempFuser: Learning Tactical and Agile Flight Maneuvers in Aerial Dogfights using a Long Short-Term Temporal Fusion Transformer

Hyunki Seong^{*1} and David Hyunchul Shim¹

Abstract—Aerial dogfights necessitate understanding the tactically changing maneuvers from a long-term perspective, along with the rapidly changing aerodynamics from a short-term view. In this paper, we propose a novel long short-term temporal fusion transformer (TempFuser) for a policy network in aerial dogfights. Our method uses two LSTM-based input embeddings to encode long-term, sparse state trajectories, as well as short-term, dense state trajectories. By integrating the two embeddings through a transformer encoder, the method subsequently derives end-to-end flight commands for agile and tactical maneuvers. We formulate a deep reinforcement learning framework to train our TempFuser-based policy model. We then extensively validate our model, demonstrating that it outperforms other baseline models against a diverse range of opponent aircraft in a high-fidelity environment. Our model successfully learns basic fighter maneuvers, human pilot-like tactical maneuvers, and robust supersonic pursuit in low altitudes without explicitly coded prior knowledge. Videos are available at <https://sites.google.com/view/tempfuser>

I. INTRODUCTION

Air-to-air combat is the tactical art of maneuvering a fighter agent to reach a position to aim at an opponent. It is also known as dogfighting, as in most cases, each fighter jet pursues the tail of the other in short-range combat situations. Dogfights have three key challenging features: 1) They are highly interactive, constantly evolving situations where each agent attempts to maximize its positional advantage. 2) They are scenarios that require tactics and accuracy to place a high-speed opponent in a tight effective damage range. 3) They take place in a three-dimensional aerial environment governed by complex aerodynamics, with safety altitude restrictions to avoid crashes to the ground.

For successful dogfights, the agent requires a combination of situational awareness, strategic planning, and maneuverability from long and short-term perspectives. Firstly, the agent has to plan its tactical position by understanding the opponent’s long-term trajectories. Naive chasing after the adversary’s immediate positions may provide a temporary advantage, but it can eventually leave itself in a vulnerable position later. Therefore, the agent should constantly assess the opponent’s long-term maneuvers, react to their actions, and strategically position itself to gain an advantage over the adversary. Secondly, the agent needs to have the ability to comprehend the agile maneuverability of the aircraft from



Fig. 1: Our approach controls the F-16 (right) to win against an opponent in a high-fidelity flight simulation, DCS.

a short-term dynamics perspective. Modern fighter jets are engineered to possess high maneuverability, enabling them to swiftly alter direction and speed, resulting in rapid changes in the engagement situation. Therefore, in order to maintain an advantageous position against the opponent, the agent should promptly grasp both the opponent’s agile movements and the agent’s own potential maneuvers from a dynamic perspective.

To handle those challenges, conventional approaches design rule-based policies that employ appropriate Basic Fighter Maneuvers (BFMs) derived from human pilot experience [1]–[3]. However, they require complex handcrafted rule sets and rely heavily on heuristics for choosing proper flight maneuvers. This leads to a lack of generality for various aircraft and combat policies. On the other hand, modern deep learning-based approaches, especially those based on deep reinforcement learning (DRL), implement complex policies through data-driven and experience-based schemes [4]–[10]. Without supervision of expert demonstrations, DRL allows for the optimization of policies through environment interactions using reward functions. However, despite the success of numerous traditional network models in aerial applications, developing a policy network that can effectively understand and execute strategic maneuvers of high-speed fighter jets still remains a challenge.

In this paper, we propose *TempFuser*, a transformer-based [11] policy network that integrates long and short-term temporal trajectory representations to learn tactical and agile flight maneuvers in dogfights. The network utilizes two separate LSTMs to extract features of the overall flight maneuvers and instantaneous dynamical transitions from the corresponding temporal state trajectory inputs. Additionally, a transformer encoder extracts global contexts from the

This research was supported by a research program (No. UE191120RD) through the Agency for Defence Development.

^{*}Corresponding author

¹Hyunki Seong and David Hyunchul Shim are with the School of Electrical Engineering, Korea Advanced Institute of Science and Technology, Daejeon, South Korea. hynkis@kaist.ac.kr, hcshim@kaist.ac.kr

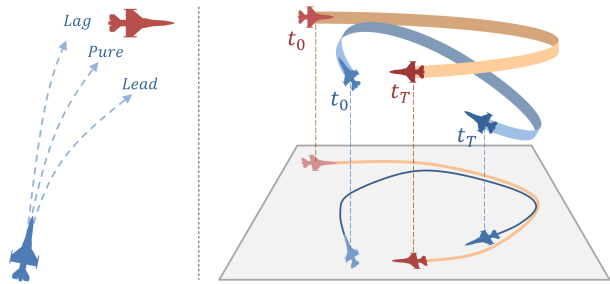


Fig. 2: Examples of tactical maneuvers: Pursuit strategies (left) and an out-of-plane maneuver, Low Yo-Yo (right).

temporal features, which reflect the opponent’s tactical and dynamical characteristics. By integrating these distinct perspectives into the inference of the policy network, TempFuser enables agents to gain a comprehensive understanding of the tactical situation in agile dogfight scenarios and execute strategic flight controls to defeat the opponent.

We tackle the aerial dogfight problem with DRL in the Digital Combat Simulator (DCS) [12], considered one of the most authentic and realistic simulation environments for fighter aircraft. DCS offers a unique platform for configuring a wide range of high-quality aircraft and airborne scenarios. We formulate the dogfighting problem as a reinforcement learning framework and design a reward function that can learn strategic dogfight maneuvers. We extensively train and validate our network with various opponent aircraft, such as F-15E, F-16, F/A-18A, and Su-27. As a result, we demonstrate that TempFuser learns challenging flight maneuvers in an end-to-end manner and outperforms various opponent aircraft, including those with superior specifications. Additionally, it exhibits robust pursuit performance at low altitudes and high-speed flight scenarios above Mach 1. The summary of our paper is as follows:

- Design of a novel long short-term temporal fusion network, TempFuser; and
- Formulation of a DRL framework including reward function for learning tactical and agile maneuvers; and
- Extensive evaluation of our agent against diverse types of opponent aircraft in a high-fidelity environment, demonstrating tactical flight maneuvers, winning against superior-spec aircraft, and robust supersonic pursuit.

II. RELATED WORKS

A. Conventional Approaches

In dogfights, human pilots typically aim to enter the opponent’s maneuver plane, which is an osculating plane where the opponent’s turn circle occurs. They use lead/pure/lag pursuit strategies to reduce the angle of deviation and keep the desired distance without overshooting. However, challenges may arise in maintaining an attack position due to variances in energy levels or aircraft performance. To overcome these challenges, pilots also employ *the out-of-plane maneuver* in which they intentionally deviate from the opponent’s maneuver plane and utilize gravity assist to improve their horizontal turning performance (such as the

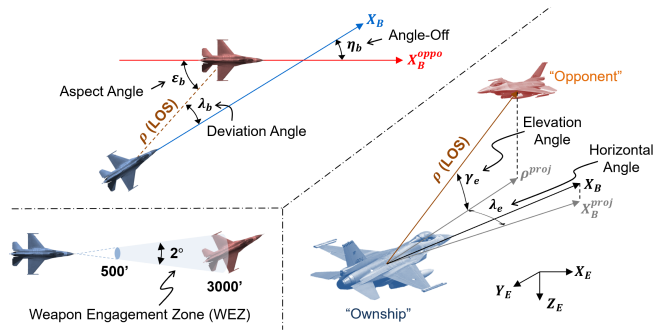


Fig. 3: Geometries for aerial dogfights.

Low Yo-Yo in Fig. 2). These tactical strategies enable pilots to convert altitude and velocity, redistribute potential and kinetic energy, and optimize flight maneuvers [13].

Based on human pilot tactics, most of the conventional studies use rule-based heuristics as a design approach. They proposed guidance laws with BFMs for the selection of pursuit strategies [1], [2] and offensive/defensive maneuvers [3] in air-to-air combat. Although heuristic-based methods are efficient in practice, they often suffer from the need for manual adjustment of parameters and flexibility issues in complex dynamic aerial environments. Several theoretical approaches utilize optimization methods, such as approximate dynamic programming (ADP) or differential game. The ADP provides a fast response by efficiently approximating the optimal policy [14]. The differential game method uses a scoring function matrix to generate optimal maneuvers [15]. However, these methods often require a finite action representation for real-time computation, which is not suitable for maneuvering in a large action space.

B. Learning-based Approaches

Recent DRL-based studies can be categorized into two parts: hierarchical and end-to-end approaches.

Hierarchical approaches involve a hierarchical structure with a high-level policy and a low-level controller. The policy infers discretized high-level actions in terms of maneuvers or tactics, while the controller computes low-level commands based on the actions. These methods construct a maneuver library [4]–[6] or multiple sub-policies [7] to choose proper flight maneuvers and strategies based on the current context of the combat geometry. Despite their efficient policy optimization within a small search space, they are limited to predefined discrete maneuvers and handcrafted strategies, resulting in a lack of generality.

On the other hand, end-to-end methods directly map the combat geometry-based state representations into flight control actions. They design MLP [8], [9] or LSTM-based network models [10], enabling policy learning using experiential data and reward functions without dependencies or limitations imposed by prior knowledge. However, it still remains a challenge to develop a policy network architecture that can comprehend the agile features of fighter jets with their tactical maneuvers and learn human pilot-like skills without explicit prior knowledge.

III. COMBAT GEOMETRIES

The geometrical relationships between the aircraft in dogfights are illustrated in Fig. 3. For simplicity, the ego and opponent aircraft are referred to as the ownship and the opponent, respectively. The line-of-sight (LOS) vector ρ denotes a vector from the ownship to the opponent. The deviation and aspect angle (λ_b, ϵ_b) represent the angle between ρ and each heading vector of the ownship (X_b) and opponent (X_b^{oppo}), respectively. The angle-off η_b indicates the angular difference between the heading vector of the ownship and opponent. We further define the horizontal and elevation angles (λ_E, γ_E) that represent the horizontal and vertical deviation angles that can be obtained from Eq. 1:

$$\gamma_e = \cos^{-1} \left[\frac{\rho \cdot \rho^{proj}}{|\rho| |\rho^{proj}|} \right], \lambda_e = \cos^{-1} \left[\frac{X_b^{proj} \cdot \rho^{proj}}{X_b^{proj} |\rho^{proj}|} \right], \quad (1)$$

where the superscript *proj* indicates a projected vector with respect to the global plane XY_E . In air combat research, the geometric area where the agent can effectively inflict damage is defined as the weapon engagement zone (WEZ), which is a two-degree spherical cone truncated at a distance range of 500 to 3000 ft from the ego aircraft [7].

IV. METHODOLOGIES

A. State and Action Representation

The state space is represented by three elements: x_t^{own}, x_t^{oppo} and a_{t-1} . $x_t^{own} \in \mathbb{R}^{13}$ has aircraft aerodynamic states of the ownship as follows:

$$x_t^{own} = \{v_x^b, a_x^b, a_z^b, \phi_b, \theta_b, \dot{\phi}_b, \dot{\theta}_b, \dot{\psi}_b, \alpha_b, \beta_b, E, z_e, v_z^e\} \quad (2)$$

where v_x^b is the true airspeed which is aligned with the axis of the relative wind in aircraft. a_x^b, a_z^b are the longitudinal and vertical acceleration, and ϕ_b, θ_b are the roll and pitch angle in the body frame. $\dot{\phi}_b, \dot{\theta}_b, \dot{\psi}_b$ denote the rate of the roll, pitch, and yaw angle. α_b and β_b indicate the angle of attack (AoA) and side slip angle. $E = z_e + (v_x^b)^2 / (2g)$ represents the specific energy of the ownship, where z_e is the altitude and g is the gravitational acceleration. v_z^e is the vertical velocity in the earth frame. Another state element $x_t^{oppo} \in \mathbb{R}^{16}$ has geometric and dogfight-related state variables as

$$x_t^{oppo} = \{P_e^{bo}, P_b^{bo}, O_b^{bo}, \lambda_b, \epsilon_b, \eta_b, \lambda_e, \gamma_e, \xi_{own}, \xi_{oppo}\} \quad (3)$$

where $P_e^{bo} \in \mathbb{R}^3$ and $P_b^{bo} \in \mathbb{R}^3$ denote the opponent's relative position in the earth and body frame, respectively, $O_b^{bo} \in \mathbb{R}^3$ indicates the opponent's relative orientation with respect to the body frame. ξ_{own}, ξ_{oppo} refer to the life scores of the ownship and opponent. All the state elements are normalized to $[-1, 1]$. We also append the previous action $a_{t-1} \in \mathbb{R}^4$ to the state so that our policy can incorporate the state and past action to infer the underlying dynamics of the ownship. The combined features $x_t = \{x_t^{own}, x_t^{oppo}, a_{t-1}\}^T$ result in a 33D state space.

The action space is represented by four control commands:

$$a_t = \{u_\phi, u_\theta, u_\psi, u_\tau\} \quad (4)$$

where $u_\phi, u_\theta, u_\psi, u_\tau$ specify the aileron, elevator, rudder, and thrust commands of the ownship in continuous space.

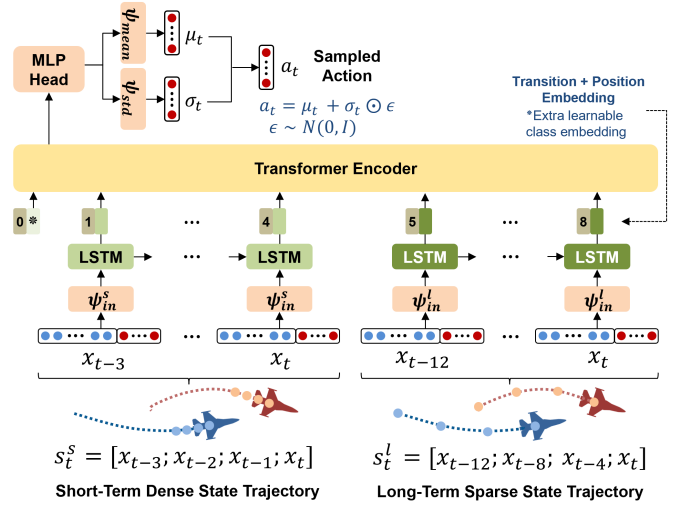


Fig. 4: Overview of the TempFuser architecture for the policy network with the following example sets $n_s = n_l = \Delta t = 4$.

B. Long Short-Term Temporal Fusion Network

A schematic illustration of the TempFuser is shown in Fig. 4. We first configure long and short-term state trajectories to represent tactical and dynamical state transitions. The short-term dense temporal trajectory, $s_t^s \in \mathbb{R}^{n_s \times 33}$, is a state history of length n_s with single-step resolution that includes the current state x_t . Since s_t^s has the same time resolution as the environment, the dense state trajectory represents the dynamic state transition information. (Eq. 5). On the other hand, the long-term sparse state trajectory, $s_t^l \in \mathbb{R}^{n_l \times 33}$, is a state history of length n_l with multi-step resolution Δt that includes the current state x_t . It has different state transitions from aircraft dynamics, representing overall maneuver-perspective features (Eq. 6). In this study, we set $n_s = n_l = \Delta t = 8$ to obtain trajectories of sufficient length to extract maneuver-level features.

$$s_t^s = [x_{t-(n_s-1)}; x_{t-(n_s-2)}; \dots; x_{t-1}; x_t] \quad (5)$$

$$s_t^l = [x_{t-(n_l-1)\Delta t}; x_{t-(n_l-2)\Delta t}; \dots; x_{t-\Delta t}; x_t] \quad (6)$$

To handle different temporal representations, s_t^s, s_t^l , we employ two LSTM-based input embedding pipelines. We first encode each temporal representation through a linear layer $\psi_{in}^i \in \mathbb{R}^{33 \times d}$, $i = \{l, s\}$ with ReLU nonlinearity. We then sequentially process each encoded trajectory feature with its corresponding LSTM. This generates hidden outputs for each trajectory, which we configure as a temporal input embedding (Eq. 7). By employing two separate LSTMs, we incorporate the sequential relational inductive bias [16] associated with both dense and sparse state transitions into the input state trajectories. As a result, the agent extracts not only the instantaneous physical properties but also the comprehensive features of the maneuvers from observations.

As all layers use the same layer size d , the two pipelines encode the input trajectories to long and short-term transition embeddings, $h_l \in \mathbb{R}^{n_l \times d}$ and $h_s \in \mathbb{R}^{n_s \times d}$, respectively.

$$h_i = \text{LSTM}(\text{ReLU}(\psi_{in}^i(s_t^i))), \quad i = \{l, s\} \quad (7)$$

We leverage a transformer encoder [11] that can learn global context to fuse two distinct transition embeddings. Before feeding the embeddings into the encoder, we concatenate them into a single sequential embedding and prepend a learnable class token $z_{class} \in \mathbb{R}^{1 \times d}$. This token serves as a one-dimensional representation vector to summarize the sequence input and represent information about the multi-temporal state transition. Additionally, we add another learnable position embedding $z_{pos} \in \mathbb{R}^{(n_l+n_s+1) \times d}$ to the sequential embedding to provide a positional feature for each element (Eq. 8).

$$z_0 = [z_{class}; h_l^1; h_l^2; \dots; h_l^{n_l}; h_s^1; h_s^2; \dots; h_s^{n_s}] + z_{pos} \quad (8)$$

Following [11], the transformer encoder consists of a multi-head self-attention (MSA) block and an MLP block, as well as layer normalizations (LN) and residual connections (Eq. 9, 10). The MLP has two FC layers with GeLU activation. The encoders are stacked L times, increasing the capacity of the transformer network. The first element in the output of the last encoder (z_L^0), corresponding to the class token, is derived as the final output $y \in \mathbb{R}^d$ through another MLP head composed of a linear layer and LN (Eq. 11).

$$z'_k = \text{MSA}(\text{LN}(z_{k-1})) + z_{k-1}, \quad k = 1, \dots, L \quad (9)$$

$$z_k = \text{MLP}(\text{LN}(z'_k)) + z'_k, \quad k = 1, \dots, L \quad (10)$$

$$y = \text{MLP}(\text{LN}(z_L^0)) \quad (11)$$

TempFuser computes the action $a_t \in \mathbb{R}^4$ in continuous space using a squashed Gaussian policy [17]. The mean and standard deviation of the action μ_t, σ_t are computed through linear projections $\psi_{mean}, \psi_{std} \in \mathbb{R}^{d \times 4}$, respectively (Eq. 12). During training, a stochastic action is sampled from these two values using the reparameterization trick of the Gaussian policy [18]. During evaluation, only the mean is used to derive a deterministic action. We use a nonlinear squashing function (tanh) for the action to be bounded within a finite range of $[-1, 1]$ (Eq. 13).

$$\mu_t = \psi_{mean}(\text{LN}(y)), \quad \sigma_t = \psi_{std}(\text{LN}(y)) \quad (12)$$

$$a_t = \tanh(\mu_t + \sigma_t \odot \xi), \quad \xi \sim N(0, I). \quad (13)$$

C. Soft Actor-Critic with State Trajectories

We construct an actor-critic architecture to optimize our policy network, following the Soft Actor-Critic (SAC) incorporating the clipped double-Q trick [17]. We set the TempFuser-based policy π_ϕ , parameterized by ϕ , as the actor. Additionally, we configure two Q-function networks Q_{θ_1} and Q_{θ_2} , parameterized by θ_1 and θ_2 , respectively, as the critics. The Q-network has the LSTM-based pipelines similar to those of the policy model. However, for model efficiency, it uses a residual block [19] containing two linear layers, instead of the transformer structure. The Q-value is computed using two additional linear projections. All of the linear layers in the critic network use ReLU nonlinearity. After the input embedding process, the critic concatenates the terminal values of the hidden outputs from the two LSTMs, as well as the action a_t . The concatenated vector is then fed into the MLP block to compute a Q-value.

Algorithm 1 SAC Training Algorithm with State Trajectories

Input: ϕ, θ_1, θ_2

Output: Optimized parameters ϕ, θ_1, θ_2

```

1:  $\bar{\theta}_1 \leftarrow \theta_1, \bar{\theta}_2 \leftarrow \theta_2, D \leftarrow \emptyset, \mathcal{T}^\dagger \leftarrow \emptyset$ 
2: for each episode do
3:   while  $n_l \Delta t$  steps do
4:     Execute action  $a_{init}$  and observe  $x_{t+1}^{own}, x_{t+1}^{oppo}, r_t$ 
5:      $\mathcal{T}.enqueue(\{x_{t+1}^{own}, x_{t+1}^{oppo}, a_{init}\})$ .
6:     while not done do
7:        $s_t^s \leftarrow \{\mathcal{T}[n_l \Delta t - (n_s - 1)]; \mathcal{T}[n_l \Delta t - (n_s - 2)]; \dots;$ 
          $\mathcal{T}[n_l \Delta t - 1]; \mathcal{T}[n_l \Delta t]\}$ 
8:        $s_t^l \leftarrow \{\mathcal{T}[\Delta t]; \mathcal{T}[2\Delta t]; \dots; \mathcal{T}[(n_l - 1)\Delta t]; \mathcal{T}[n_l \Delta t]\}$ 
9:        $a_t \sim \pi_\phi(a_t | s_t^s, s_t^l)$ 
10:      Execute action  $a_t$  and observe  $x_{t+1}^{own}, x_{t+1}^{oppo}, r_t$ 
11:       $\mathcal{T}.dequeue()$  and  $\mathcal{T}.enqueue(\{x_{t+1}^{own}, x_{t+1}^{oppo}, a_t\})$ 
12:       $s_{t+1}^s \leftarrow \{\mathcal{T}[n_l \Delta t - (n_s - 1)]; \mathcal{T}[n_l \Delta t - (n_s - 2)]; \dots;$ 
         $\mathcal{T}[n_l \Delta t - 1]; \mathcal{T}[n_l \Delta t]\}$ 
13:       $s_{t+1}^l \leftarrow \{\mathcal{T}[\Delta t]; \mathcal{T}[2\Delta t]; \dots; \mathcal{T}[(n_l - 1)\Delta t]; \mathcal{T}[n_l \Delta t]\}$ 
14:       $D \leftarrow D \cup \{(s_t^s, s_t^l, a_t, r_t, s_{t+1}^s, s_{t+1}^l)\}$ 
15:      for each gradient step do
16:         $\theta_i \leftarrow \theta_i - \lambda_Q \nabla_{\theta_i} J_Q(\theta_i)$  for  $i \in \{1, 2\}$ 
17:         $\phi \leftarrow \phi - \lambda_\pi \nabla_\phi J_\pi(\phi)$ 
18:         $\alpha \leftarrow \alpha - \lambda_\alpha \nabla_\alpha J_\alpha(\alpha)$ 
19:         $\bar{\theta}_i \leftarrow \tau \theta_i + (1 - \tau) \bar{\theta}_i$  for  $i \in \{1, 2\}$ 

```

[†]The index of \mathcal{T} is started from 1.

SAC is an off-policy algorithm that is sample efficient and robust with respect to hyperparameter tuning. It optimizes the policy π_ϕ by maximizing a trade-off between the expected return and the entropy of the policy with a temperature parameter α . The critic networks are updated by the clipped double Q-learning with delayed target Q-networks $Q_{\bar{\theta}_j}$ to mitigate the overestimation and stabilize the learning process of the critics.

Algorithm 1 summarizes the overall training process. At the beginning of each episode, a fixed-size FIFO buffer \mathcal{T} is initialized with $n_l \Delta t$ states that are observed by actions a_{init} in the environment. In each step, the long and short-term state trajectories s_t^l and s_t^s are indexed from the buffer \mathcal{T} . The state trajectories are then fed to the policy π_ϕ and an action a_t is sampled to interact with the environment. After the agent observes the next states $x_{t+1}^{own}, x_{t+1}^{oppo}$ and reward r_t , the oldest state is dequeued and $x_{t+1} = \{x_{t+1}^{own}, x_{t+1}^{oppo}, a_t\}$ is enqueued in \mathcal{T} . New state trajectories are indexed from the updated buffer and the transition data $(s_t^s, s_t^l, a_t, r_t, s_{t+1}^s, s_{t+1}^l)$ is stored into a replay buffer D . During the update phase, The model parameters θ_1, θ_2 and ϕ with the temperature α are updated with the objective functions $J_Q(\theta_1), J_Q(\theta_2), J_\pi(\phi)$ and $J_\alpha(\alpha)$. The weight of the target Q-functions $\bar{\theta}_1$ and $\bar{\theta}_2$ are updated by Polyak Averaging [20] with a coefficient τ .

D. Reward Function and Termination Rule

The reward function r_t is a weighted combination of the following seven reward terms (Table I):

Energy-Pursuit Score (r_1): r_1 encourages the agent to minimize angular error with the opponent and place the opponent within the desired distance range, while managing its energy during maneuvers. This term consists of a pursuit score function f_p (Fig. 6) and a factor κ determined by the specific energy E . The score function assigns higher scores



Fig. 5: **Left** : Aerial scenario configurations for training and evaluation. **Right** : Different types of aircraft for the opponent.

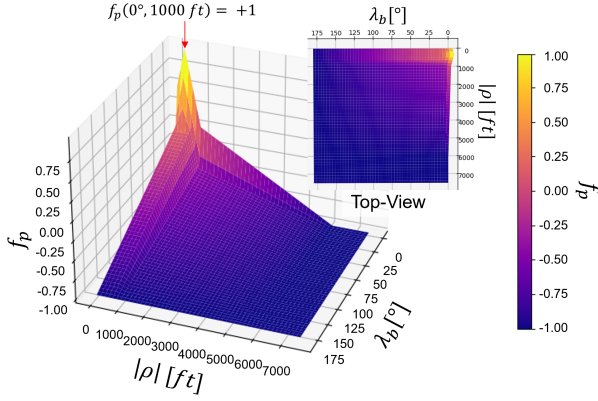


Fig. 6: Illustration of the pursuit score function.

to deviation angles (λ) closer to zero and relative distances ($|\rho|$) closer to the desired distance of 1000 ft inside the WEZ. On the contrary, the function outputs lower scores for larger λ values and relative distances farther from 1000 ft. κ is determined by the sign of f_p and scales the magnitude of r_1 by \bar{E} , which is the value of E normalized to the specific energy at the maximum speed of 800 kt and altitude of 30 000 ft. This energy-embedded pursuit score motivates the agent to maintain sufficient specific energy when tracking an opponent, and to learn maneuvers that minimize energy loss by managing potential and kinetic energy.

Horizontal Pursuit (r_2): To enhance the pursuing performance in terms of the horizontal component, we define a reward term r_2 to minimize the horizontal angle λ_e .

WEZ (Ownship, Opponent) (r_3, r_4): r_3 is calculated as a sparse positive reward if the LOS vector ρ is in the ownship's spherical cone-shaped WEZ (WEZ_{own}), which decreases the opponent's life score ξ_{oppo} by 1. Similarly, r_4 is calculated as a sparse negative feedback when ρ is in the opponent's WEZ (WEZ_{oppo}), which reduces ownship's score ξ_{own} by 1. All agents have a life of 20 at the beginning, and the episode is terminated when any agent loses all of its score.

Altitude (r_5): r_5 prevents the agent from maneuvering below the minimum allowable altitude $z_{min} = 250$ ft. To create dense reward signals, we set a low altitude threshold $z_{low} = 1000$ ft and continuously penalize the agent whenever its altitude z is below it. We also increase the penalty proportionally to the magnitude of the vertical speed (v_z) to motivate the agent to slow down its descent at the moment of impact [21]. If any agent drops below z_{min} , it is considered to have crashed down and the episode is terminated.

TABLE I: Reward terms for aerial dogfights.

Reward Terms	Reward Functions
Energy-Pursuit Score	$r_1 = \kappa f_p(\lambda_b, \rho)$, $\kappa = \begin{cases} (1.5 - \bar{E}) & f_p < 0 \\ (0.5 + \bar{E}) & f_p \geq 0 \end{cases}$
Horizontal Pursuit	$r_2 = -\lambda_e/180^\circ$
WEZ (Ownship)	$r_3 = \begin{cases} +1 & \rho \in WEZ_{own} \\ 0 & \rho \notin WEZ_{own} \end{cases}$
WEZ (Opponent)	$r_4 = \begin{cases} -1 & \rho \in WEZ_{oppo} \\ 0 & \rho \notin WEZ_{oppo} \end{cases}$
Altitude	$r_5 = 0.5(1 + \min(v_z, 0)) \left(\min\left(0, \frac{z - z_{low}}{z_{low} - z_{min}}\right) \right)^3$
AoA	$r_6 = \begin{cases} - \alpha_b /45^\circ & \alpha_b < 0^\circ \\ 0 & 0^\circ \leq \alpha_b < 45^\circ \\ -(\alpha_b - 45^\circ)/45^\circ & \alpha_b \geq 45^\circ \end{cases}$
Specific Energy	$r_7 = clip((E - E_{des})/E_{des}, -1, +1)$

AoA (r_6): r_6 penalizes the agent when its AoA (α_b) is outside the range of 0-45 degrees, discouraging maneuvers that decrease lift forces and result in an aerodynamic stall.

Specific Energy (r_7): r_7 encourages the agent to maintain a specific energy E that is close to a desired value E_{des} defined by a target speed (400 kt) and altitude (15 000 ft).

V. EXPERIMENT

A. Environment Setup

We configure dogfight scenarios using DCS that has high-fidelity flight dynamics and a range of mission configuration tools. We select the F-16 for our agent, which is an example of a mature fighter jet. Fig. 5 (left) shows the scenario configurations. In training episodes, our agent (illustrated by a blue point) is initialized with an altitude of 15 000 ft and a speed of 500 kt, and the opponent, with different altitudes (10 000–18 000 ft), is randomly spawned with various locations (illustrated by red points) within 30 000 ft from our agent. In the evaluation, the agent and opponent are spawned facing each other at a distance of 10 000 ft, engaging in episodes that enable fair performance comparisons.

Different fighter jets for the opponents are illustrated in Fig. 5 (right). Four aircraft are randomly spawned as an opponent in the training episode: F-16, an equivalent aircraft to our agent, F-15E and F/A-18A, which have comparable specs, and Su-27, which has better aerodynamic performance than our agent aircraft. In addition to the four aircraft, we additionally spawn the Su-30, which has not been encountered during training, to validate the robustness of our policy against the new opponent in the evaluation phase. For more details about the aircraft, we refer the reader to [22].

TABLE II: Quantitative Evaluation against 4 Opponents (F-15E, F-16, F/A-18, Su-27) and an Unseen Aircraft (Su-30)

Method	v.s. F-15E				v.s. F-16				v.s. F/A-18				v.s. Su-27				v.s. Su-30			
	Win (%) \uparrow	Lose (%) \downarrow	Damage (%) \uparrow	Life (%) \uparrow	Win (%) \uparrow	Lose (%) \downarrow	Damage (%) \uparrow	Life (%) \uparrow	Win (%) \uparrow	Lose (%) \downarrow	Damage (%) \uparrow	Life (%) \uparrow	Win (%) \uparrow	Lose (%) \downarrow	Damage (%) \uparrow	Life (%) \uparrow	Win (%) \uparrow	Lose (%) \downarrow	Damage (%) \uparrow	Life (%) \uparrow
DCS-Ace	34.6	43.0	38.9	54.4	38.3	39.6	38.8	59.1	18.7	58.0	32.9	32.3	22.9	41.8	37.0	52.7	9.2	66.4	19.2	28.6
MLP	37.3	58.5	38.2	40.2	3.7	87.6	4.6	10.1	6.5	85.1	8.2	10.8	1.7	31.3	3.8	53.3	5.7	72.4	7.3	20.0
LSTM	88.6	10.9	91.8	89.0	28.6	64.2	38.5	34.9	83.8	15.4	88.5	79.4	55.7	35.3	67.2	60.0	60.4	39.3	71.3	58.5
LS-LSTM	83.3	16.7	86.7	78.2	75.6	20.1	83.2	77.5	88.1	11.7	90.8	87.0	82.6	14.4	85.9	77.0	62.4	36.8	69.7	60.3
TempFuser	93.5	6.5	94.2	92.5	86.3	13.4	96.0	86.6	89.1	10.9	90.3	86.2	92.5	7.0	95.1	92.0	86.1	13.9	90.8	81.2

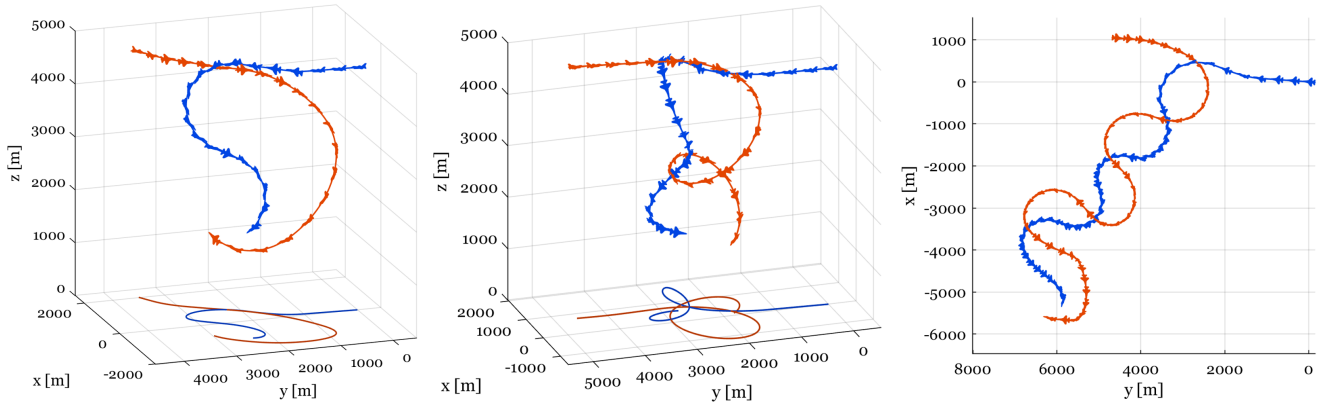


Fig. 7: Results of engagements against the opponent (left: F-15E, middle: F-16, right: Su-27). 3D flight and horizontally projected trajectories of the ownship (blue) and opponent (red) are illustrated from the beginning until the winning moment.

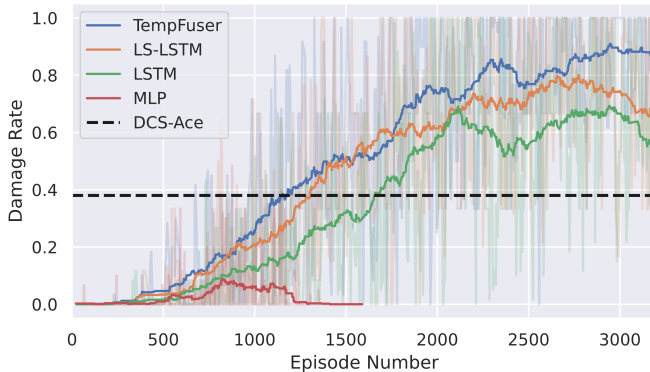


Fig. 8: Learning curves of the normalized damage rate against the opponent.

B. Evaluation

We performed the performance evaluation of our transformer-based policy, TempFuser, and conducted a comparison with four other baseline models: DCS-Ace, MLP, LSTM, and LS-LSTM. DCS-Ace is a built-in AI with the highest pilot skill, *Ace*, in the DCS simulator. The remaining baseline models are all learnable models trained by SAC, similar to our policy model. However, their state representation and network architecture are different. The MLP is a multilayer perceptron network that observes only the current state x_t . The LSTM receives a short-term state trajectory s_t^s based on an LSTM layer. The LS-LSTM incorporates both long and short-term trajectories (s_t^l, s_t^s) but consists only of LSTM layers without the transformer encoder.

1) *Learning curves*: We evaluated learning curves across different policies using the WEZ damage ratio. This ratio sig-

nifies the proportion of the opponent’s life that our agent has reduced through the use of WEZ. By assessing this metric once every 10 episodes, we can quantify the improvement in performance over the course of training. Fig. 8 compares the performance of different baseline policies. The results show that our model surpasses other baseline models in terms of performance convergence and learning speed. The MLP was unable to learn the appropriate maneuvers to confront aggressive opponents. While the LSTM successfully learned aerial dogfights and achieved a damage rate of over 50%—a rate higher than that of the DCS-Ace—its performance plateaued at around 60%. By employing the long and short-term features, the LS-LSTM exhibited better performance compared to the LSTM. However, as it only concatenates these two features without adequately integrating them, it failed to fully leverage their combined potential, preventing it from surpassing the 80% performance threshold. Incorporating the transformer architecture, TempFuser effectively captured the opponent’s tactical and dynamic attributes, allowing an average 90% WEZ damage.

2) *Quantitative Performance*: Table II summarizes the performance of the different policies against four types of aircraft, as well as an unseen aircraft, the Su-30. We applied four metrics for the quantitative evaluation: win rate (Win), lose rate (Lose), WEZ damage rate (Damage), and the life score of the ownship (Life). All the metrics are averaged after each episode. Our model generally outperforms other baseline models in terms of win and damage rates against different opponent aircraft. Among the baseline models, the non-learning DCS-Ace often fell short of reaching the end game (win or lose) and struggled to defeat fighters with

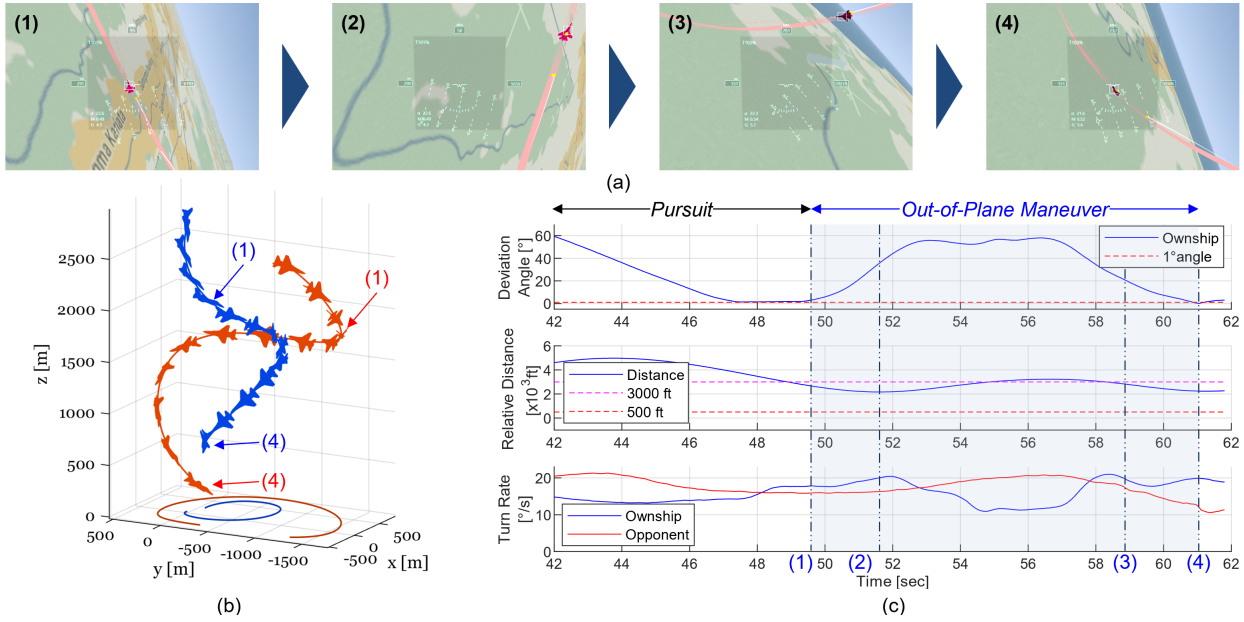


Fig. 9: Learned tactical out-of-plane maneuver (similar to Low Yo-Yo) against a superior-spec aircraft (Su-30). (a) Snapshots of the pilot’s view while (1-4); (b) Ownship (blue) and opponent (red) trajectories while (1-4); (c) Overall quantitative error, distance, and turn rate results in the episode.

higher aerodynamic specifications, such as the Su-27 and Su-30. When it comes to the learnable models, the F-16 and Su-27/30 aircraft present the greatest challenge as an opponent. In these scenarios, the ownship is not able to utilize the performance difference between the aircraft based on their aerodynamic specifications. Only the policy models that incorporate both long and short-term trajectory inputs (LS-LSTM, TempFuser) demonstrate remarkable successes, achieving a win/damage rate of over 50% against the various types of opponents, including those challenging aircraft. However, the performance of the LS-LSTM was notably diminished when encountering the unobserved opponent (Su-30), leading to a significant decrease in win/damage rates to around 60%. Our TempFuser method, on the other hand, exhibits only a minor performance decrement while effectively reducing the opponent’s life score by an average of 90%, achieving the highest win rate (86%) and life rate (81%).

C. Learned Flight Behavior

1) *Basic flight maneuvers*: Fig. 7 shows the flight trajectories of our agent against the three different opponents (F-15E, F-16, Su-27) during aerial dogfights. The overall results show that our method learned the basic maneuverability of fighter jets and successfully performed faster turning maneuvers through complex combinations of the four control commands to track the opponent. Fig. 7 (left) illustrates the result of an episode against an F-15E opponent. While the opponent performed with an average turn rate of $7.85^\circ/\text{s}$ (max. $16.80^\circ/\text{s}$), our agent showed a more rapid average turn rate of $11.18^\circ/\text{s}$ (max. $26.41^\circ/\text{s}$), enabling it to quickly gain a favorable position and outperform the enemy agent.

Furthermore, our agent understands the opponent’s complex turns and responds to them with strategic reactive

behaviors. Fig. 7 (middle) depicts an engagement with the F-16 opponent, which is the same aircraft as our agent. When the opponent performed two turning descents, our agent responded by executing a spiral dive with a tighter radius and faster turning speed, eventually winning the engagement by targeting the anticipated area where the enemy was expected to reach. As another scenario, Fig. 7 (right) shows the results of engaging an aggressive opponent, the Su-27. With superior aerodynamic performance than the F-16, it is capable of executing high-speed complex maneuvers, making pursuit challenging. In response, our TempFuser-based agent showed *Flat Scissors*-like maneuvers [13] against the enemy aircraft, crossing the opponent’s trajectory and effectively aiming the fast-moving target aircraft.

2) *Tactical flight maneuvers*: Without explicit prior knowledge, our method discovers and learns tactical maneuvers that are close to the human pilot’s skills depicted in Fig. 2. Fig. 9 shows the results of an engagement situation with a Su-30 opponent. Our agent executed pursuit maneuvers until 49.7 sec, reducing the tracking error and relative distance by up to 1.4° and 2621 ft (Fig. 9 (1)). However, the pursuit method alone was not able to place the Su-30, which has a faster average speed of 496 kt (919 km/h), in the effective damage zone of our F-16. To overcome this situation, our agent changed its tactics to the out-of-plane maneuver that leveraged gravity assist to make a rapid turn towards the expected path of the opponent, despite the increased tracking angle error (Fig. 9 (1-4)). Those tactical maneuvers enabled our agent to stay within the opponent’s turning circle while keeping the distance within 500–3000 ft, even against the faster opponent. Moreover, our agent achieved a more rapid instantaneous turn rate ($20.97^\circ/\text{s}$) than the opponent, strategically placing it within our agent’s WEZ (Fig. 9 (4)).

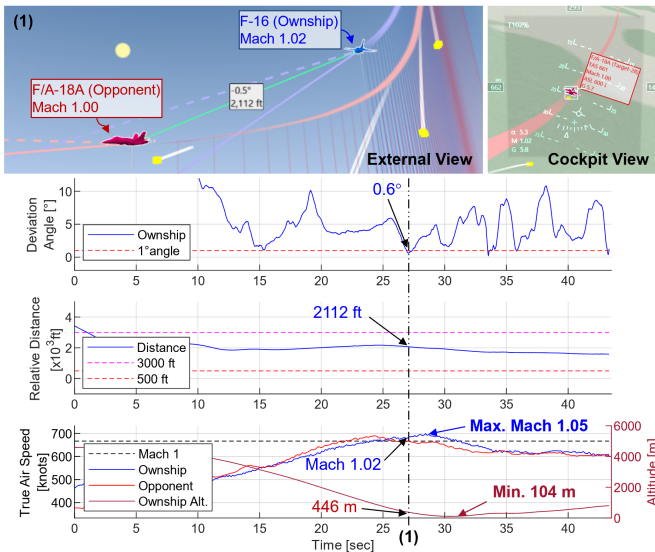


Fig. 10: Quantitative results of a scenario that crosses subsonic and supersonic speeds against the F/A-18A opponent.

3) *Robust pursuit in supersonic speed:* We further investigated the robustness of the policy in aggressive scenarios, specifically at supersonic speeds. Fig. 10 illustrates an aerial scene with overall quantitative results where our agent tracked an F/A-18A opponent evading to a low altitude with near-supersonic velocity. As the deviation angle decreased, the opponent increased its speed by descending to an altitude below 500 ft. Against such a high-speed adversary, our agent maintained the desired distance while traveling at Mach 1.02 and reduced the deviation angle by up to 0.6° . It then executed high-speed pursuit up to Mach 1.05 at a critically low altitude while keeping the proper distance within the WEZ range (near 2000 ft). Finally, it won against the adversary by accumulating damage. These results show the robustness of our policy model to aim the agile opponent in supersonic situations with considering safe altitude requirements.

VI. CONCLUSION

We introduce a long short-term temporal fusion network (TempFuser) that utilizes a transformer-based architecture for aerial dogfights. Our method integrates both long-term and short-term trajectory representations to effectively capture the maneuverability and dynamic-level features of agile fighter jets engaged in aggressive aerial combat scenarios. In high-fidelity combat scenarios, our proposed model demonstrates superior performance when compared to other baseline methods, across a diverse range of opponent aircraft types. Our model successfully learns robust pursuit and tactical out-of-plane maneuvers without heuristic knowledge.

We believe our work has potential for broader applications beyond dogfights. It could be extended to other agile and interactive scenarios, such as autonomous racing, where understanding the strategies of other aggressive agents is crucial. In future work, we aim to adapt our method to these fields, as well as to enhance our method for use in multi-agent scenarios over the one-versus-one context.

REFERENCES

- [1] G. H. Burgin and L. Sidor, "Rule-based air combat simulation," Tech. Rep., 1988.
- [2] N. Ramírez López and R. Żbikowski, "Effectiveness of autonomous decision making for unmanned combat aerial vehicles in dogfight engagements," *Journal of Guidance, control, and Dynamics*, vol. 41, no. 4, pp. 1021–1024, 2018.
- [3] H. Shin, J. Lee, H. Kim, and D. H. Shim, "An autonomous aerial combat framework for two-on-two engagements based on basic fighter maneuvers," *Aerospace Science and Technology*, vol. 72, pp. 305–315, 2018.
- [4] Q. Yang, J. Zhang, G. Shi, J. Hu, and Y. Wu, "Maneuver decision of uav in short-range air combat based on deep reinforcement learning," *IEEE Access*, vol. 8, pp. 363–378, 2019.
- [5] Z. Fan, Y. Xu, Y. Kang, and D. Luo, "Air combat maneuver decision method based on a3c deep reinforcement learning," *Machines*, vol. 10, no. 11, p. 1033, 2022.
- [6] J. Hu, L. Wang, T. Hu, C. Guo, and Y. Wang, "Autonomous maneuver decision making of dual-uav cooperative air combat based on deep reinforcement learning," *Electronics*, vol. 11, no. 3, p. 467, 2022.
- [7] A. P. Pope, J. S. Ide, D. Mićović, H. Diaz, D. Rosenbluth, L. Ritholtz, J. C. Twedt, T. T. Walker, K. Alcedo, and D. Javorsek, "Hierarchical reinforcement learning for air-to-air combat," in *2021 international conference on unmanned aircraft systems (ICUAS)*. IEEE, 2021, pp. 275–284.
- [8] W. Kong, D. Zhou, Z. Yang, K. Zhang, and L. Zeng, "Maneuver strategy generation of ucav for within visual range air combat based on multi-agent reinforcement learning and target position prediction," *Applied Sciences*, vol. 10, no. 15, p. 5198, 2020.
- [9] J. Yoo, H. Seong, D. H. Shim, J. H. Bae, and Y.-D. Kim, "Deep reinforcement learning-based intelligent agent for autonomous air combat," in *2022 IEEE/AIAA 41st Digital Avionics Systems Conference (DASC)*. IEEE, 2022, pp. 1–9.
- [10] J. H. Bae, H. Jung, S. Kim, S. Kim, and Y.-D. Kim, "Deep reinforcement learning-based air-to-air combat maneuver generation in a realistic environment," *IEEE Access*, vol. 11, pp. 26427–26440, 2023.
- [11] A. Dosovitskiy, L. Beyer, A. Kolesnikov, D. Weissenborn, X. Zhai, T. Unterthiner, M. Dehghani, M. Minderer, G. Heigold, S. Gelly *et al.*, "An image is worth 16x16 words: Transformers for image recognition at scale," *arXiv preprint arXiv:2010.11929*, 2020.
- [12] Eagle Dynamics, "Digital combat simulator world," 2023. [Online]. Available: <https://www.digitalcombatsimulator.com>
- [13] R. L. Shaw, "Fighter combat," *Tactics and Maneuvering*; Naval Institute Press: Annapolis, MD, USA, 1985.
- [14] J. S. McGrew, J. P. How, B. Williams, and N. Roy, "Air-combat strategy using approximate dynamic programming," *Journal of guidance, control, and dynamics*, vol. 33, no. 5, pp. 1641–1654, 2010.
- [15] H. Park, B.-Y. Lee, M.-J. Tahk, and D.-W. Yoo, "Differential game based air combat maneuver generation using scoring function matrix," *International Journal of Aeronautical and Space Sciences*, vol. 17, no. 2, pp. 204–213, 2016.
- [16] P. W. Battaglia, J. B. Hamrick, V. Bapst, A. Sanchez-Gonzalez, V. Zambaldi, M. Malinowski, A. Tacchetti, D. Raposo, A. Santoro, R. Faulkner *et al.*, "Relational inductive biases, deep learning, and graph networks," *arXiv preprint arXiv:1806.01261*, 2018.
- [17] T. Haarnoja, A. Zhou, K. Hartikainen, G. Tucker, S. Ha, J. Tan, V. Kumar, H. Zhu, A. Gupta, P. Abbeel *et al.*, "Soft actor-critic algorithms and applications," *arXiv preprint arXiv:1812.05905*, 2018.
- [18] J. Schulman, N. Heess, T. Weber, and P. Abbeel, "Gradient estimation using stochastic computation graphs," *arXiv preprint arXiv:1506.05254*, 2015.
- [19] K. He, X. Zhang, S. Ren, and J. Sun, "Deep residual learning for image recognition," in *Proceedings of the IEEE conference on computer vision and pattern recognition*, 2016, pp. 770–778.
- [20] B. T. Polyak and A. B. Juditsky, "Acceleration of stochastic approximation by averaging," *SIAM journal on control and optimization*, vol. 30, no. 4, pp. 838–855, 1992.
- [21] H. Seong, C. Jung, S. Lee, and D. H. Shim, "Learning to drive at unsignalized intersections using attention-based deep reinforcement learning," in *2021 IEEE International Intelligent Transportation Systems Conference (ITSC)*. IEEE, 2021, pp. 559–566.
- [22] A. Bongers and J. L. Torres, "Measuring technological trends: A comparison between us and ussr/russian jet fighter aircraft," *Technological Forecasting and Social Change*, vol. 87, pp. 125–134, 2014.